PCCP

PAPER

View Article Online
View Journal | View Issue

Cite this: *Phys. Chem. Chem. Phys.*, 2016, **18**, 18855

Fullerenol $C_{60}(OH)_{16}$ prevents amyloid fibrillization of $A\beta_{40}$ – *in vitro* and *in silico* approach†

Zuzana Bednarikova,‡[ab] Pham Dinh Quoc Huy,‡[cf] Maria-Magdalena Mocanu,[d] Diana Fedunova,[a] Mai Suan Li*[c] and Zuzana Gazova*[ae]

Received 9th February 2016,
Accepted 17th June 2016

DOI: 10.1039/c6cp00901h

www.rsc.org/pccp

The generation of Aβ amyloid aggregates in the form of senile plaques in the brain is one of the pathological hallmarks of Alzheimer's disease (AD). There is no cure for AD and one of the recent treatment strategies is focused on the inhibition of amyloid fibrillization of Aβ peptide. Fullerene C_{60} has been proposed as a candidate for destroying Aβ aggregates but it is not soluble in water and its toxicity to cells remains largely ambiguous. To overcome these drawbacks, we synthesized and studied the effect of water-soluble fullerenol $C_{60}(OH)_{16}$ (fullerene C_{60} carrying 16 hydroxyl groups) on the amyloid fibrillization of $A\beta_{40}$ peptide *in vitro*. Using a Thioflavin T fluorescent assay and atomic force microscopy it was found that $C_{60}(OH)_{16}$ effectively reduces the formation of amyloid fibrils. The IC_{50} value is in the low range (μg ml^{-1}) suggesting that fullerenol interferes with $A\beta_{40}$ aggregation at stoichiometric concentrations. The *in silico* calculations supported the experimental data. It was revealed that fullerenol tightly binds to monomer $A\beta_{40}$ and polar, negatively charged amino acids play a key role. Electrostatic interactions dominantly contribute to the binding propensity *via* interaction of the oxygen atoms from the COO^- groups of side chains of polar, negatively charged amino acids with the OH groups of fullerenol. This stabilizes contact with either the D23 or K28 of the salt bridge. Due to the lack of a well-defined binding pocket fullerenol is also inclined to locate near the central hydrophobic region of $A\beta_{40}$ and can bind to the hydrophobic C-terminal of the peptide. Upon fullerenol binding the salt bridge becomes flexible, inhibiting Aβ aggregation. In order to assess the toxicity of fullerenol, we found that exposure of neuroblastoma SH-SY5Y cells to fullerenol caused no significant changes in viability after 24 h of treatment. These results suggest that fullerenol $C_{60}(OH)_{16}$ represents a promising candidate as a therapeutic for Alzheimer's disease.

Introduction

The misfolding of proteins that leads to the formation of amyloid aggregates plays an important role in many different human diseases. Aβ peptides, the proteolytic by-products of amyloid precursor protein cleavage, are usually composed of 39–43 amino acid residues and might undergo conformational changes to form amyloid structures rich in β-sheet motifs. Aβ amyloid fibrillar structures accumulated in the form of senile plaques in the brain are one of the pathological hallmarks of Alzheimer's disease (AD). There is no cure for AD and one of the recent treatment strategies is focused on decreasing the production of Aβ.[1] The other strategy is based on the inhibition of the Aβ peptide self-assembly amyloid fibrillization or clearance of the existing amyloid plaques.[2] Several small molecules,[3–6] short peptides[7,8] or nanoparticles[9–12] were identified as effective inhibitors of Aβ peptide amyloid fibrillization *in vitro*.

In recent years, the fullerenes due to their unique spherical structure[13] have become known for their antioxidant, neuroprotective, cytoprotective and antitumor properties.[14,15] Moreover, they might be used as carriers of contrast agents, radiopharmaceuticals or drugs, and are thus promising tools with applications in medical diagnostics and therapy.[16] However, the poor solubility of fullerenes in polar solvents restricts their use as

[a] *Department of Biophysics, Institute of Experimental Physics, Slovak Academy of Sciences, Watsonova 47, 040 01 Kosice, Slovakia. E-mail: gazova@saske.sk*
[b] *Department of Biochemistry, Institute of Chemistry, Faculty of Science, Safarik University, Srobarova 2, 041 54 Kosice, Slovakia*
[c] *Institute of Physics, Polish Academy of Sciences, Al. Lotnikow 32/46, 02-668 Warsaw, Poland. E-mail: masli@ifpan.edu.pl*
[d] *Department of Biophysics, "Carol Davila" University of Medicine and Pharmacy, 050474 Bucharest, Romania*
[e] *Department of Medical and Clinical Biochemistry, Faculty of Medicine, Safarik University, Trieda SNP 1, 040 11 Kosice, Slovakia*
[f] *Institute for Computational Science and Technology, SBI building, Quang Trung Software City, Tan Chanh Hiep Ward, District 12, Ho Chi Minh City, Vietnam*
† Electronic supplementary information (ESI) available. See DOI: 10.1039/c6cp00901h
‡ These authors contributed equally.

biomedicine agents.[17] Therefore, a great effort is focused on modification of fullerenes to increase their solubility in water solutions. These derivatives are usually prepared by addition of different polar functional groups to the carbon cage. Attachment of hydroxyl groups leads to the formation of water soluble forms named fullerenols or fullerols [$C_{60}(OH)_n$]. These have been shown to absorb oxygen radical species, which can attack lipids, proteins, DNA, and other macromolecules. Fullerenols with high solubility and the ability to cross the blood brain barrier have been described as excellent antioxidants, reducing apoptosis in cortical neuron cultures.[18] Fullerenol derivatives have also been reported as potential inhibitors of HIV-1 protease[19] or as anti-cancer agents.[20]

Several water soluble fullerene derivatives have been described as having the ability to interfere with amyloid aggregation of proteins. Kim and Lee have shown that the 1,2-(dimethoxylmethano)fullerene derivative inhibits amyloid fibrillization of $A\beta_{40}$ and its fragment $A\beta_{11-25}$ in the early stages of aggregation.[21] Electron microscopy has revealed that hydrated C_{60} fullerene (C_{60}HyFn) suppressed the aggregation of $A\beta_{25-35}$ and $A\beta_{42}$.[22] Bobylev *et al.* also studied the effect of several water-soluble C_{60} fullerene nitroderivatives,[23] $C_{60}Cl(C_6H_4CH_2COONa)_5$, and polyvinyl pyrrolidone derivatives[23–25] on amyloid fibrillization of $A\beta_{42}$ peptide and X-protein as well as their ability to destroy mature fibrils.

The potential utilization of fullerenols for biomedical applications raises the question of their biocompatibility. Several *in vitro* studies have determined the dose-responsive, time-, cell line- and hydroxylation-dependent effect of fullerenols on cell viability. Johnson-Lyles *et al.* have shown that fullerenol at concentrations lower than 6 mM was nontoxic for a porcine proximal tubule cell model – LLC-PK1 cells.[26] Su *et al.* assessed the cytotoxic effect of fullerenol in the tenth to hundreds of μg ml^{-1} range on Chinese hamster lung and ovary cells, but found almost no effect on L929 mouse subcutaneous connective cells.[27] The effect of fullerenols with various degrees of hydroxylation on human epidermal keratinocyte viability was also reported. The fullerenol was nontoxic up to 8.5 μg ml^{-1} regardless of the hydroxylation degree. At higher concentrations of fullerenol, toxicity occurred for the most hydroxylated fullerenols.[28] Zha *et al.* have shown that fullerenol can increase the viability of hippocampal neurons and protect them against oxidative risk, as well as promoting cell death, depending on the applied concentration.[29]

In this paper we studied the interaction between the amyloid fibrillization of $A\beta_{40}$ peptide and fullerenol $C_{60}(OH)_{16}$, a water-soluble form of fullerene C_{60} carrying approximately 16 hydroxyl groups. A Thioflavin T fluorescent assay and atomic force microscopy have shown that fullerenol inhibits the formation of $A\beta_{40}$ amyloid aggregates *in vitro*. The *in silico* data obtained by molecular mechanics Poisson–Boltzmann surface area (MM-PBSA) methods showed that fullerenol tightly binds to monomer $A\beta_{40}$, supporting the experimental data. For fullerenol binding, the electrostatic interactions are the most important; and the key role is played by polar, negatively charged amino acids. In order to assess the toxicity of fullerenol, we found that exposure of neuroblastoma SH-SY5Y cells to fullerenol caused no significant changes in viability at 24 h of treatment.

Experimental

Chemicals

$A\beta_{1-40}$ peptide ($A\beta_{40}$) (Cat # A-1001-2, Lot # 10290940T) was obtained from rPeptide (USA). Powder fullerene C_{60} (379646-1G) was purchased from Sigma-Aldrich. Thioflavin T (ThT), NaOH, 3-(*N*-morpholino)-propanesulfonic acid (MOPS), DMSO and NaN_3 were obtained from Sigma Aldrich and were of analytical reagent grade. All other chemicals were purchased from Sigma Aldrich or Fluka and were of analytical reagent grade.

Preparation of water-soluble fullerenol

Fullerenol, a polyhydroxylated derivative of fullerene was prepared by a Solvent Free Reaction described by Wang *et al.*[30] Briefly, fullerene C_{60} was mixed with H_2O_2 and NaOH under grinding conditions in air at room temperature. This provides water-soluble fullerenol with ~16 hydroxyl group bonded to the carbon scaffold ($C_{60}(OH)_{16}$). The Fourier transform infrared spectroscopy (FTIR) spectrum of $C_{60}(OH)_{16}$ (Fig. S1, ESI†) showed broad hydroxyl absorption at 3106 cm^{-1}, C=C absorption at 1609 cm^{-1} and C–O stretching absorption at 1098 cm^{-1}. These data are in accordance with spectra of $C_{60}(OH)_{16}$ fullerenol published by Wang *et al.*[30]

In vitro amyloid fibrillization of $A\beta_{40}$ peptide

$A\beta_{40}$ amyloid fibrils were prepared by dissolving the peptide to a stock concentration of 665 μM in 10 mM NaOH solution. UV-vis spectroscopy (JASCO V-630) was used to determine peptide concentration using an extinction coefficient of $\varepsilon_{292} = 2300\ M^{-1}\ cm^{-1}$. The solution was sonicated for 1 min in a bath sonicator and then centrifuged for 10 min (12 000*g*) at 4 °C to precipitate the large aggregates. After centrifugation the concentration was measured again. The stock solution of $A\beta_{40}$ was diluted to a final concentration of 10 μM in 150 mM 3-(*N*-morpholino)-propanesulfonic acid (MOPS) solution with pH 6.9 and incubated for 7 days at 37 °C. Formation of amyloid aggregates was observed by Thioflavin T assay and confirmed by atomic force microscopy.

Thioflavin T (ThT) assay

Fibrillization of $A\beta_{40}$ peptide was detected as a significant enhancement of the ThT fluorescence intensity. ThT was added to the $A\beta_{40}$ samples (10 μM) to a final concentration of 20 μM. Measurements were performed in a 96-well plate using a Synergy MX (BioTek) spectrofluorimeter. The excitation was set at 440 nm and the emission recorded at 485 nm. The excitation and emission slits were adjusted to 9.0/9.0 nm and the top probe vertical offset was 6 mm.

In vitro interference of the fullerenol $C_{60}(OH)_{16}$ and $A\beta_{40}$ peptide amyloid fibrillization; determination of the IC_{50} value

The ability of fullerenol to affect amyloid fibrillization of the $A\beta_{40}$ peptide was first investigated at three different $A\beta_{40}$: $C_{60}(OH)_{16}$ concentration ratios (w/w), namely 100 : 1, 20 : 1 and 1 : 1 using ThT assay; the peptide concentration was 10 μM corresponding 43.3 μg ml^{-1}. For control experiments the peptide was replaced with buffer to measure the fluorescence of fullerenol, which was

comparable to the fluorescence detected for native $A\beta_{40}$ peptide. The IC_{50} value represents concentration of fullerenol inducing 50% inhibition of $A\beta_{40}$ amyloid fibrillization. The ability of fullerenol (at a concentration range 0.06–4330 μg ml^{-1}) to inhibit formation of $A\beta_{40}$ amyloid aggregates (10 μM peptide concentration) was determined using ThT assay. The fluorescence intensities of samples obtaining fullerenol were normalized to the fluorescence signal of amyloid aggregates alone. The IC_{50} values were determined from the curves obtained by fitting of the average fluorescence values with sigmoidal function – Logistic, Parameter 3 in the SigmaPlot software (Systat Software Inc., USA) using the equation $y = a/(1 + (x/x_0)^b)$, where x_0 corresponds to IC_{50} value. Each experiment was performed in triplicate and the final value represents the average of measured values.

Atomic force microscopy (AFM)

Samples were placed by drop casting on the freshly cleaved mica surface. After 5 min adsorption, the samples were washed with ultrapure water and left to dry. AFM images were taken using a Scanning Probe Microscope (Veeco di Innova, Bruker AXS Inc., Madison, USA) in a tapping mode using an NCHV cantilever with specific resistance of 0.01–0.025 Ω cm, antimony (n) doped Si, radius of the tip curvature of 10 nm. The resolution of image was 512 pixels per line (512 × 512 pixels per image) and the scan rate 0.25–0.5 kHz. No smoothing or noise reduction was applied.

Cell culture and viability assay

The neuroblastoma cell line SH-SY5Y was obtained from the company German Collection of Microorganisms and Cell Culture (DSMZ, Germany) and was grown according to their specifications. Briefly, the cells were grown in Dulbecco's Modified Eagle Medium (DMEM) (Sigma Aldrich) supplemented with 20% fetal bovine serum (Sigma Aldrich), 100 I.U. ml^{-1} penicillin/100 μg ml^{-1} streptomycin (Sigma Aldrich), 2 mM L-glutamine (Sigma Aldrich), while for the sub-culturing (twice/week) the cells were seeded at the concentration of 1×10^6 cells per 75 cm^2. For the viability assay, SH-SY5Y cells were seeded in triplicate at a density of 7×10^3 cells per sample in 96-well flat-bottom microplates 24 h prior to the experiments, followed by incubation with fullerenol. The viability assay was performed in triplicate using a cell proliferation reagent WST-1 (Roche Diagnostics GmbH, Mannheim, Germany), based on the reduction of tetrazolium salt 4-[3-(4-iodophenyl)-2-(4-nitrophenyl)-2*H*-5-tetrazolio]-1,3-benzene disulfonate (WST-1) to formazan by mitochondrial dehydrogenases. The absorbance of formazan was measured at 450 nm and corrected at 620 nm using a 96-well spectrophotometer (ELISA plate reader).

Treatment of the cells with fullerenol

For the treatments with $C_{60}(OH)_{16}$ fullerenol the SH-SY5Y cells were seeded in 96-well plates and incubated for 24 and 72 h with 0.001, 0.005, 0.05, 0.5, 5, 50 μg ml^{-1} fullerenol. All the incubation steps were carried out in complete medium and after the corresponding incubation time the WST-1 viability assay was performed.

In silico experiments

Choice for structure of fullerenol $C_{60}(OH)_{16}$. First we tried to find the most stable structure of $C_{60}(OH)_{16}$, *i.e.* the distribution of 16 hydroxyl (OH) around the C_{60} fullerene buckyball with the lowest energy. This task is not easy as there are many possible configurations. On the other hand, it has been shown that for $C_{60}(OH)_{24}$ an energetically favorable conformation can be obtained by locating OH groups on the equator of the C_{60} surface.[31] Following this strategy we have studied seven isomers named as L1, L2, L3, L4, L5, L6 and L7 (Fig. 1) showing that, in agreement with He *et al.*,[31] isomer L1 with OH groups regularly positioned on the equator of the C_{60} surface has the lowest energy (Table S1 in ESI†). Here the energy of the isomers was calculated in the Hartree–Fock approximation implemented in Gaussian.[32] L2 has the lowest stability compared to L1 due to the equatorial distribution of the OH groups. Isomer L7, in which the hydroxyls are uniformly distributed around the buckyball, has the highest energy. In L3–L6 the distributions of OH groups are not symmetric relative to the two poles of the C_{60} cage. The stability ranking based on the energy is L1 > L2 > L3 > L4 > L5 > L6 > L7. To access convergence of results we studied L1 and L7, which have the highest and lowest stability from the chosen set, by both docking and MD simulations, while the binding of other isomers to $A\beta_{40}$ were examined by the docking method.

Parameterization of fullerenol $C_{60}(OH)_{16}$. In our simulation, the attachment of 16 hydroxyl (OH) groups to C_{60} fullerene buckyball was carried out using GaussView 05.[33] Prior to deriving the force-field parameters for a classical Molecular Dynamic (MD) simulation, the structure of fullerenol was optimized by the Hartree–Fock method using the basis set 6-31G* implemented in Gaussian 09.[34] Parameters that are compatible with force-field AMBER99SB[35] and GAFF[36] were generated by AmberTool[37] with the AM1-BCC charge model.[38]

Docking method

Since Aβ peptides are intrinsically disordered in water, their PDB structures are not available. Therefore, structures used as targets for molecular docking have been generated by molecular dynamics all-atom simulations. For the $A\beta_{40}$ monomer we used five representative structures (Fig. 5) produced in our previous works.[39]

AutodockTools 1.5.4[40] and Autodock Vina 1.1[41] were used to prepare necessary files and then to search for energetically

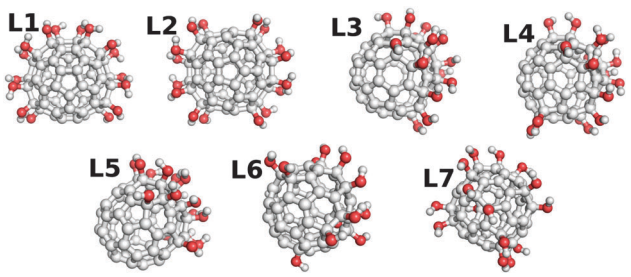

Fig. 1 Optimized configurations of the 7 $C_{60}(OH)_{16}$ isomers. The stability ranking is L1 > L2 > L3 > L4 > L5 > L6 > L7.

favorable binding positions of fullerenol to $A\beta_{40}$. Because the binding sites of $A\beta_{40}$ are not *a priori* available the docking box should cover the whole peptide. The box was centered at the center of $A\beta_{40}$, with grid dimensions chosen as large as $28.2 \times 31.0 \times 38.4$ Å^3. During docking simulations the $A\beta_{40}$ peptide was kept rigid, while the ligand was allowed to freely flex all of its torsional degrees of freedom and the exhaustiveness was set to 400 which is good enough to produce reliable results.

Molecular mechanics Poisson–Boltzmann surface area (MM-PBSA) method and MD simulation

The docking method has the advantage that it can make an accurate prediction of the binding location of small molecules in proteins. However, because it adopts a semi-empirical scoring function and several crude approximations, like the omission of receptor dynamics and a limited number of ligand trial positions, it usually fails to provide a good estimation of the binding energy and delineate binding mechanisms. Thus, the binding affinity was refined using a more accurate MM-PBSA method. In this method, snapshots produced in MD equilibrium simulations are employed to compute the free energy of the ligand binding to the receptor. The binding free energy ΔG_{bind} obeys the following equation:

$$\begin{aligned}\Delta G_{\text{bind}} &= G_{\text{receptor–ligand}} - G_{\text{free receptor}} - G_{\text{free ligand}} \\ &= \Delta E_{\text{vdW}} + \Delta E_{\text{ele}} + \Delta G_{\text{PB}} + \Delta G_{\text{sur}} - T\Delta S \qquad (1)\end{aligned}$$

Here $\Delta G_{\text{receptor–ligand}}$, $\Delta G_{\text{free receptor}}$, and $\Delta G_{\text{free–ligand}}$ are contributions from the complex, free receptor, and free ligand, respectively. The van der Waals (vdW) (ΔE_{vdW}) and electrostatic (ΔE_{ele}) interactions were calculated using the Lennard-Jones and charge parameters (Tables S2 and S3 in the ESI†) generated for the MD simulation. Polar (ΔG_{PB}) and non-polar (ΔG_{sur}) solvent-mediated interactions were estimated using the package PBSA included in AmberTools. The former term can be obtained by solving the Poisson–Boltzmann equation,[42,43] while the latter is defined by solvent accessible surface area (SASA) weighted by an empirical surface tension coefficient $g = 0.005$ plus a cavity offset constant, which was set equal 0. The entropy S was estimated by normal mode analysis with the help of the program mmpbsa_py_nabnmode included in AmberTools.

To obtain snapshots for computing ΔG_{bind}, the MD simulation was carried out using the TIP3P water model,[44] AMBER99SB[35] and GAFF[36] force fields. The simulation was done using the Amber12 package[45] and the details of the simulation process are available in our previous work.[46] For each model of $A\beta_{40}$ with fullerenol we performed two different MD runs starting from the same configuration but with different velocity fields. The lengths of the ten trajectories varied from 160 to 800 ns (τ_{total}) depending on the equilibration time (τ_{eq}) of isomers. More details about the MD simulation can be found in Tables S2 and S3 in ESI.†

Tools and measures used in the structure analysis

The $A\beta_{40}$–fullerenol interaction was monitored by the contact map. The side-chain contact between $A\beta_{40}$ and fullerenol formed if the distance between the center of mass side chain of a given $A\beta_{40}$ residue and the nearest atom of fullerenol became smaller than 6.5 Å. Once a hydrogen bond (HB) was formed, the distance between the donor D and acceptor A was less than 3.5 Å, the H–A distance less than 2.7 Å and the D–H–A angle larger than 135 degrees.

Results

In the past decade, fullerenes have been a hot topic in the field of biomedical applications for their unique properties such as high antioxidant activity and neuroprotection.[47,48] Less attention has been drawn to the effect of fullerene and its derivatives on amyloid aggregation of proteins. We investigated the effect of fullerenol $C_{60}(OH)_{16}$, a water-soluble polyhydroxylated derivative of fullerene C_{60}, on amyloid fibrillization of $A\beta_{40}$ using *in vitro* and *in silico* methods.

Effect of fullerenol $C_{60}(OH)_{16}$ on $A\beta_{40}$ fibrillization *in vitro*

Fullerenol $C_{60}(OH)_{16}$ was prepared by the procedure described by Wang *et al.*[30] which provides fullerenol with ~16 hydroxyl groups bonded to carbon scaffold (more data in part Materials and methods and Fig. S1 in ESI†). The ability of fullerenol to affect the process of $A\beta_{40}$ amyloid fibrillization was studied by ThT fluorescence assay. After binding of ThT to amyloid structures an increase in fluorescence intensity is observed and the fluorescence signal is proportional to the amount of amyloid aggregates. In the presence of ThT, the fluorescence spectrum of $A\beta_{40}$ amyloid fibrils (Fig. 2, violet solid line) is significantly higher compared to the signal detected for native $A\beta_{40}$ monomers (Fig. 2, violet dotted line). The interference of fullerenol with $A\beta_{40}$ fibrillization was investigated at different w/w ratios of $A\beta_{40}$: $C_{60}(OH)_{16}$, namely 100 : 1, 20 : 1 and 1 : 1 with a fixed native $A\beta_{40}$ peptide concentration of 10 μM (10 μM = 43.3 μg ml^{-1}). The detected fluorescence spectra indicate that the interaction of fullerenol with $A\beta_{40}$ amyloid aggregation led to a decrease of

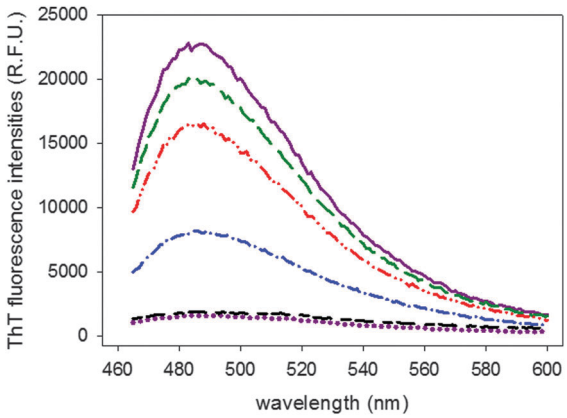

Fig. 2 ThT fluorescence spectra detected for fullerenol $C_{60}(OH)_{16}$ alone (black short dashed line), native $A\beta_{40}$ peptide before (violet dotted line) and after fibrillization alone (violet solid line) and after $A\beta_{40}$ peptide fibrillization in presence of fullerenol for $A\beta_{40}$: $C_{60}(OH)_{16}$ ratios 100 : 1 (green long dashed line), 20 : 1 (red dashed-dotted-dotted line) and 1 : 1 (blue dashed-dotted line). $A\beta_{40}$ peptide concentration was 10 μM.

fluorescence intensities with an increasing concentration of $C_{60}(OH)_{16}$ in the sample (Fig. 2). The decrease of intensity negatively correlated with the ability of fullerenol to inhibit $A\beta_{40}$ fibrillization. The highest fluorescence intensity corresponding to the lowest inhibitory activity (90%) was obtained for ratio $A\beta_{40}:C_{60}(OH)_{16}$ = 100 : 1 (Fig. 2, green long dashed line). Only a slight decrease compare to ratio 100 : 1 was detected for the ratio 20 : 1 (Fig. 2, red dashed-dotted-dotted line). ThT fluorescence decreased to intensities lower than 30% of the control sample ($A\beta_{40}$ fibrils alone) in the case of the highest fullerenol concentration (ratio 1 : 1) (Fig. 2, blue dashed-dotted line). It should be mentioned that fullerenol alone, as well as after treatment with ThT, has no fluorescence spectrum (Fig. 2, black short dashed line). Our results indicate that fullerenol is able to inhibit the formation of $A\beta_{40}$ amyloid aggregates; the extent of inhibition is determined by the fullerenol concentration.

Atomic force microscopy (AFM)

In order to visualize the inhibitory effect of fullerenol, we used atomic force microscopy (AFM). Representative AFM images of 10 μM $A\beta_{40}$ peptide after fibrillization alone or with fullerenol are shown in Fig. 3. $A\beta_{40}$ fibrillization leads to the formation of long, thin and straight fibrils with typical amyloid morphology (Fig. 3A). The final morphology of aggregates observed for fibrillization of $A\beta_{40}$ in the presence of fullerenol was depended on the concentration of fullerenol. For the w/w ratio $A\beta_{40}:C_{60}(OH)_{16}$ = 100 : 1 the amount and characteristics of the fibrils are morphologically comparable with untreated fibrils, while the amount of the fibrils is decreased (Fig. 3B). For the ratio 20 : 1 a greater reduction of fibril amount was observed; moreover, the fibrils are shorter (Fig. 3C). Interference with fullerenol at a ratio of 1 : 1 leads to extensive reduction of fibrillar aggregates (Fig. 3D) compared to fibrils produced by $A\beta_{40}$ peptide alone. The very short fibrils together with very small aggregates are observed.

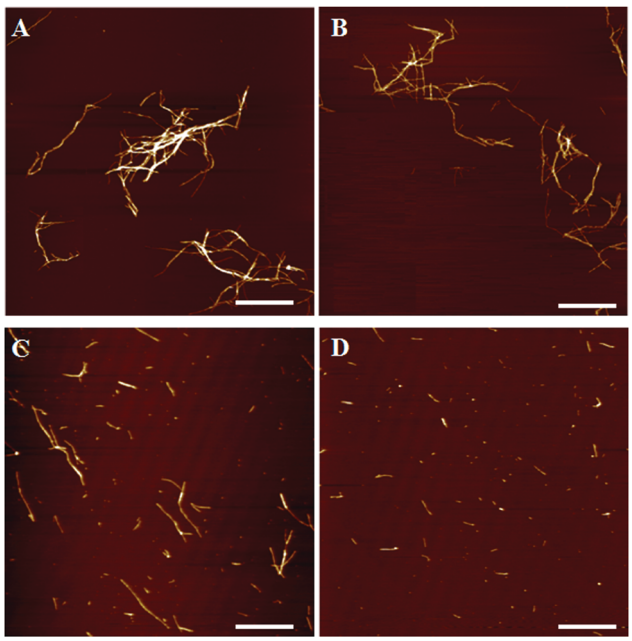

Fig. 3 AFM images of amyloid aggregates formed by 10 μM $A\beta_{40}$ alone (A) and in the presence of fullerenol at w/w ratios $A\beta_{40}:C_{60}(OH)_{16}$ = 100 : 1, 20 : 1 and 1 : 1 (B–D). Bars represent 1 μm.

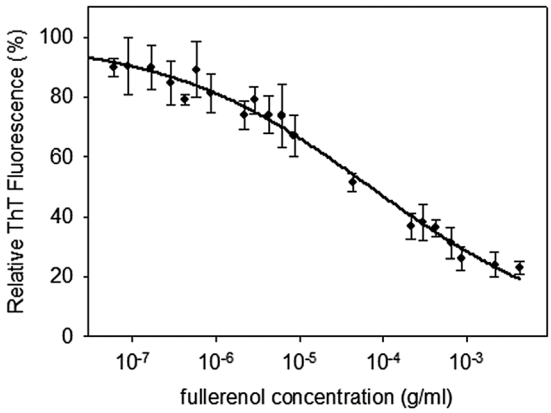

Fig. 4 The inhibiting effect of increasing fullerenol concentrations on $A\beta_{40}$ fibrillization detected by ThT assay. A single experiment was performed with each sample in triplicate. The error bars represent the average deviation for repeated measurements of three separate samples. The curve was obtained by fitting of the average values using a nonlinear least-squares method.

Determination of the IC_{50} value for the inhibiting activity of fullerenol

To quantify the inhibitory effect of fullerenol we determined the IC_{50} value the representing concentration of fullerenol causing 50% inhibition of $A\beta_{40}$ amyloid fibrillization. For this purpose, the inhibiting ability of fullerenol in concentrations varying from 0.06 to 4330 μg ml^{-1} at a fixed protein concentration (10 μM = 43.3 μg ml^{-1}) was observed by ThT assay. The observed relative fluorescence intensities normalized to the fluorescence signal of amyloid aggregates alone are shown in Fig. 4. Fullerenol inhibits the process of $A\beta_{40}$ aggregation in a dose-dependent manner. These data were fitted to calculate the concentration of fullerenol at 50% inhibition of $A\beta_{40}$ fibril formation. The determined IC_{50} value is equal to 31.9 μg ml^{-1}.

Interaction of fullerenol with $A\beta_{40}$ – *in silico* approach

To obtain more detailed information about interaction of the fullerenol with $A\beta_{40}$ peptide we studied the binding of the $C_{60}(OH)_{16}$ to the peptide. For this purpose a parameterization of fullerenol and $A\beta_{40}$ monomer was made. Fullerenol is composed of a fullerene buckyball C_{60} and 16 hydroxyl (OH) groups (Fig. 5). The 16 OH groups are bound to C_{60} in such a way that eight pairs are arranged in almost regular intervals. The number of OH groups must be even integer because each C–C double bond when changing to single one requires two OH groups to fulfil the valence balance. The structure of $A\beta_{40}$ peptide in water was not experimentally resolved because it is an intrinsically disordered peptide in an aqueous environment.[49] For molecular docking we used five representative structures (Fig. 5) generated by MD simulations in our previous work.[39]

Docking results

The binding positions obtained in the lowest energy mode for seven isomers in 5 $A\beta_{40}$ models are shown in Fig. 5. In models 1

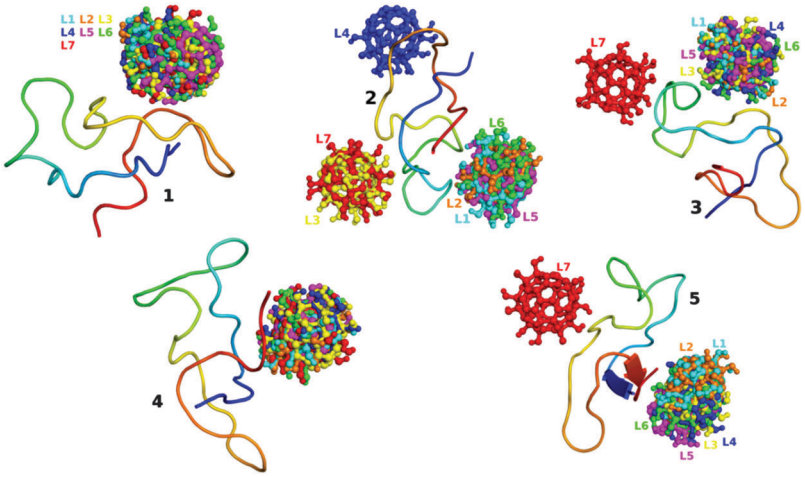

Fig. 5 Docking positions of 7 fullerenol $C_{60}(OH)_{16}$ isomers in five models of $A\beta_{40}$.

and 4, all isomers are located at the same site. In models 3 and 5 the binding site of isomer 7 is different from that of the remaining isomers. Model 2 has three main binding poses with L1, L2, L5 and L6 located together at nearly the same position. Thus, because $A\beta_{40}$ monomer in water environment has no well-defined binding site, in agreement with the previous works the fullerenol binds to different locations.[50,51]

The binding energies of the seven isomers obtained in the best docking mode in 5 models are given in Table S4 in ESI.† Clearly, within the error bars the studied isomers have the same binding energy suggesting that their impact on Aβ activity is similar. Therefore, we will focus on the most stable isomer L1 and the most unstable isomer L7.

The number of hydrogen bonds (HBs) and side-chain (SC) contacts of isomer L1 with 5 $A\beta_{40}$ models are presented in Table 1. The HBs and SC contacts are also shown in Fig. S2 in ESI† and Fig. 5, respectively. L1 forms 9 side chain contacts with different fragments of $A\beta_{40}$ including the turn region in model 1, while the location near the C-terminal is favorable for models 2, 4 and 5. In model 3 there are 8 SC contacts involving contacts with Asp23, Val24 and Gly25 from the turn and His13 and His14 in the N-terminal. Some SC contacts with the N-terminal also appeared in other models (Table 1).

The HBs and SC contact networks of isomer L7 are shown in Fig. S3 and S4 in the ESI,† respectively. The numbers of HBs and SC contacts between ligands and receptors are listed in Table S5 in the ESI.† Isomer L7 forms 11 SC contacts with different fragments of $A\beta_{40}$ in model 1, whereas the location near the turn and N-terminal is favorable for model 2. In model 3 there are only 6 SC contacts. In models 4 and 5 it prefers to locate at the same area at C-terminal but some SC contacts with the N-terminal also appeared. Thus the HBs and SC contacts networks depend on distributions of OH on the fullerene surface.

There is no correlation between the number of HBs and the binding energy ΔE_{bind} (Table 1 and Table S5, ESI†). In the case of isomer L1, model 5 has the smallest number of HBs but the absolute value of ΔE_{bind} is not the smallest one. The correlation between the binding energy and SC contacts is also absent. For instance the models 1, 2 and 5 have the same number of SC contacts of 9 but their ΔE_{bind} are different (Table 1). For isomer L7, model 4 has the lowest ΔE_{bind} but the number of HBs is not the largest one (Table S5, ESI†). The correlation between the binding energy and SC contacts is also absent. In model 1 L7 has the maximum number of SC contacts but its ΔE_{bind} is not the lowest one implying that, similar to L1, the binding energy does not correlate with the number of SC contacts.

The poor correlation between the binding affinity and the number of HB and SC contacts is probably due to crude approximations adopted in the docking method such as omission of the receptor dynamics and a finite number of trials for ligand conformations. The main advantage of the docking approach is its accurate prediction of binding sites, which are important for determining starting configurations for MD simulations.

Molecular dynamics results

We have performed MD simulations for isomers L1 and L7 interacting with Aβ. The $A\beta_{40}$–$C_{60}(OH)_{16}$ configurations obtained in the best docking modes (Fig. 5) were first solvated in water

Table 1 Binding energy ΔE_{bind} (kcal mol^{-1}), N_{hb} and N_{sc} formed by isomer L1 with five models of $A\beta_{40}$. Results were obtained by the docking method. See Fig. 5 and 6 for more information about HBs and SC contact networks

Model	ΔE_{bind}	N_{hb}	N_{sc}	Amino acids in side-chain contact with ligand
M1	−5.9	4	9	Asp1, Glu3, Ala21, Asp23, Ser26, Lys28, Ile32, Gly33, Leu34
M2	−6.7	3	9	Ser8, Tyr10, Glu11, Phe20, Val36, Gly37, Gly38, Val39, Val40
M3	−7.4	6	8	Asp7, His13, His14, Lys16, Glu22, Asp23, Val24, Gly25
M4	−7.8	4	10	Phe4, Ser8, Gly9, Tyr10, Ile31, Val36, Gly37, Gly38, Val39, Val40
M5	−6.6	2	9	Ala2, Ser8, Tyr10, Phe20, Ile31, Val36, Gly37, Gly38, Val40

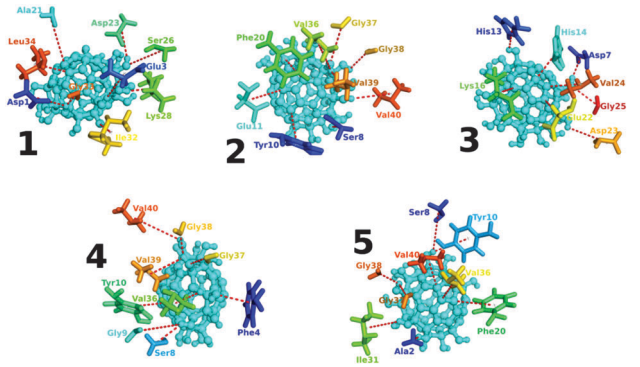

Fig. 6 Side-chain contacts between $A\beta_{40}$ and isomer L1 in the best docking poses in the 5 models (red dashed lines). The names of residues forming SC with fullerenol are explicitly shown.

and then used as starting configurations for MD simulations. For each model we generated two independent MD trajectories. The systems reach equilibrium at different time scales (τ_{eq}) when the root mean square deviation (RMSD) and the $A\beta_{40}$–$C_{60}(OH)_{16}$ interaction energy reach saturation (Fig. S5 and S6 in ESI†). The equilibration time τ_{eq}, indicated by the arrow in Fig. S5 and S6 (ESI†), varied from 32 to 630 ns. Snapshots collected every 10 ps in equilibrium (after arrow) and eqn (1) were used to calculate the binding free energy ΔG_{bind} by the MM-PBSA method.

Fullerenol $C_{60}(OH)_{16}$ strongly binds to $A\beta_{40}$

The binding free energy ΔG_{bind} of isomer L1 and L7 to $A\beta_{40}$ and its decomposed parts obtained in 10 MD runs are given in Table 2 and Table S6 in ESI,† respectively. Averaging over all 5 models with a total of 10 trajectories we obtained $\Delta G_{bind} = -18.3$ for L1 and -19.2 kcal mol^{-1} for L7. Thus, in accord with the docking results, the binding free energies are not very sensitive to stability of the isomers. Using the approximate formula $IC_{50} = \exp(\Delta G_{bind}/RT)$, where R is the gas constant and the units of IC_{50} (computational output) is mol, one can show that the inhibition constant IC_{50} of both isomers falls in the sub-nanomolar range, implying a very high binding propensity to $A\beta_{40}$.

Consistent with the docking results (Table 1), the binding affinity of isomer L1, obtained by the MM-PBSA method, is very high in model 3 and 4 (Table 2). The ranking of binding affinity of the five structure models is M4 > M3 > M5 > M2 > M1. Despite that the mean binding affinities of L1 and L7 are nearly the same, their binding free energies to individual structure models are different (compare Table 2 and Table S6 in ESI†). For models 4 and 5, where isomer L7 locates at the C-terminus, the binding is relatively weak (Table S6, ESI†). Although in the starting docking structure of model 3 L7 superficially binds to $A\beta_{40}$ with the smallest number of contacts (6 SC contacts and 0 HB), it becomes a tightest binder in both MD runs. For L7 the binding affinity of the five models is ranked as M3 > M2 > M1 > M5 > M4, which is very different from the L1 isomer.

In the presence of hydroxyl groups, in contrast to fullerenes,[46] the electrostatics contribution to ΔG_{bind} dominates over vdW and other contributions (Table 2 and Table S6, ESI†). However, hydroxyl groups themselves contribute a positive amount to the binding free energy and the main contribution to the electrostatics part comes from highly charged carbon atoms. This is consistent, for instance, with the weak binding of isomer L7 in models 4 and 5 where fullerenol binds to a highly hydrophobic region. In addition, carbon atoms dominate over OH groups in vdW interactions (Table 2 and Table S6, ESI†).

Table 2 Binding free energy (kcal mol^{-1}) of isomer L1 to $A\beta_{40}$, obtained by the MM-PBSA method. The van der Waals (ΔE_{vdW}) and electrostatic interactions for OH groups and carbon atoms (ΔE_{elec}) are in italics and bold, respectively

Model	Traj	ΔE_{vdW}		ΔE_{elec}		ΔE_{PB}	ΔE_{sur}	$-T\Delta S$	ΔG_{bind}	ΔG_{bind}
1	1	−39.3		−88.1		94.6	−3.3	25.5	−10.9 ± 5.8	−10.4
		−2.7	**−36.6**	*277.2*	**−365.3**					
	2	−44.5		−51.2		67.5	−3.4	21.8	−9.9 ± −8.0	
		−10.3	**−34.2**	*193.8*	**−225.0**					
2	1	−50.1		−87.7		107.6	−4.1	24.2	−10.3 ± 14.1	−13.5
		−6.7	**−43.3**	*239.6*	**−327.3**					
	2	−56.0		−78.8		97.1	−4.1	25.5	−16.6 ± 8.7	
		−7.8	**−48.2**	*244.4*	**−323.2**					
3	1	−65.8		−66.6		94.0	−4.4	17.7	−25.3 ± 11.5	−24.6
		−12.3	**−53.5**	*205.4*	**−271.9**					
	2	−52.4		−77.8		87.4	−4.3	23.5	−23.9 ± 8.6	
		−14.9	**−62.9**	*240.0*	**−292.4**					
4	1	−41.0		−103.0		104.7	−3.0	25.3	−17.4 ± 5.0	−27.0
		−6.9	**−34.2**	*273.3*	**−376.3**					
	2	−60.9		−123.3		122.8	−4.2	29.3	−36.6 ± 5.9	
		−0.7	**−60.2**	*319.0*	**−442.2**					
5	1	−63.7		−86.7		108.4	−4.7	27.6	−19.3 ± 11.0	−15.9
		−7.5	**−56.2**	*234.7*	**−321.5**					
	2	−31.3		−99.0		96.6	−3.1	24.7	−12.4 ± 6.5	
		1.9	**−33.2**	*259.9*	**−358.9**					
Average		−53.0		−83.7		98.1	−3.9	24.5	−18.3	

Fullerenol $C_{60}(OH)_{16}$ binds to $A\beta_{40}$ by locking to Asp23–Lys28 salt bridge and C-terminus

To shed more light on the binding mechanism the SC contact population was monitored. Fig. 7 shows the probability of isomer L1 being in contact with residues of $A\beta_{40}$ during MD simulations. In models 2, 4 and 5, where fullerenol is not inclined to bind to the C-terminus the binding mechanism might be interpreted as due to contact with this terminus. In model 1 100% of equilibrium time isomer L1 interacts with Asp23 and Lys28. In model 3 where the binding is strong (Table 2) fullerenol spends a substantial time amount near Asp23 and Lys28 (Fig. 7) suggesting that the locking to the Asp23–Lys28 salt bridge is vital for the stability of the $A\beta_{40}$–L1 complex. This is also supported by the highest mean probability to form contact with Asp23 (Fig. 7). On the other hand, in model 4 with very strong binding (Table 2) isomer L1 often interacts with the C-terminus (Fig. 7). Together with the fact that the mean propensity is high at this terminus (see also Table 3 where the list of residues that form SC contact with fullerenol more than 50% MD time is given) we conclude that the interaction with the C-terminus is also important for binding. Thus, the binding pose and mechanism depend on structure models of $A\beta_{40}$ peptide because $A\beta_{40}$, as an intrinsically disordered peptide, does not have a well-defined binding site. Fig. S7 (ESI†) shows representative snapshots where L1 forms SC contacts with the salt bridge and the C-terminus at different times.

Using snapshots collected in equilibrium from all MD trajectories we obtained the mean distance between centers of mass of Asp23 and Lys28 equal 1.02 nm which is larger than 0.83 nm computed from five $A\beta_{40}$ models shown in Fig. 5. Therefore, upon L1 binding the Asp23–Lys28 salt bridge becomes more flexible resulting in reduction of aggregation rates.[52–54]

In model 5 isomer L1 is not prone to locate near the central hydrophobic region 17–21 (LVFFA) (Fig. 7), which is important

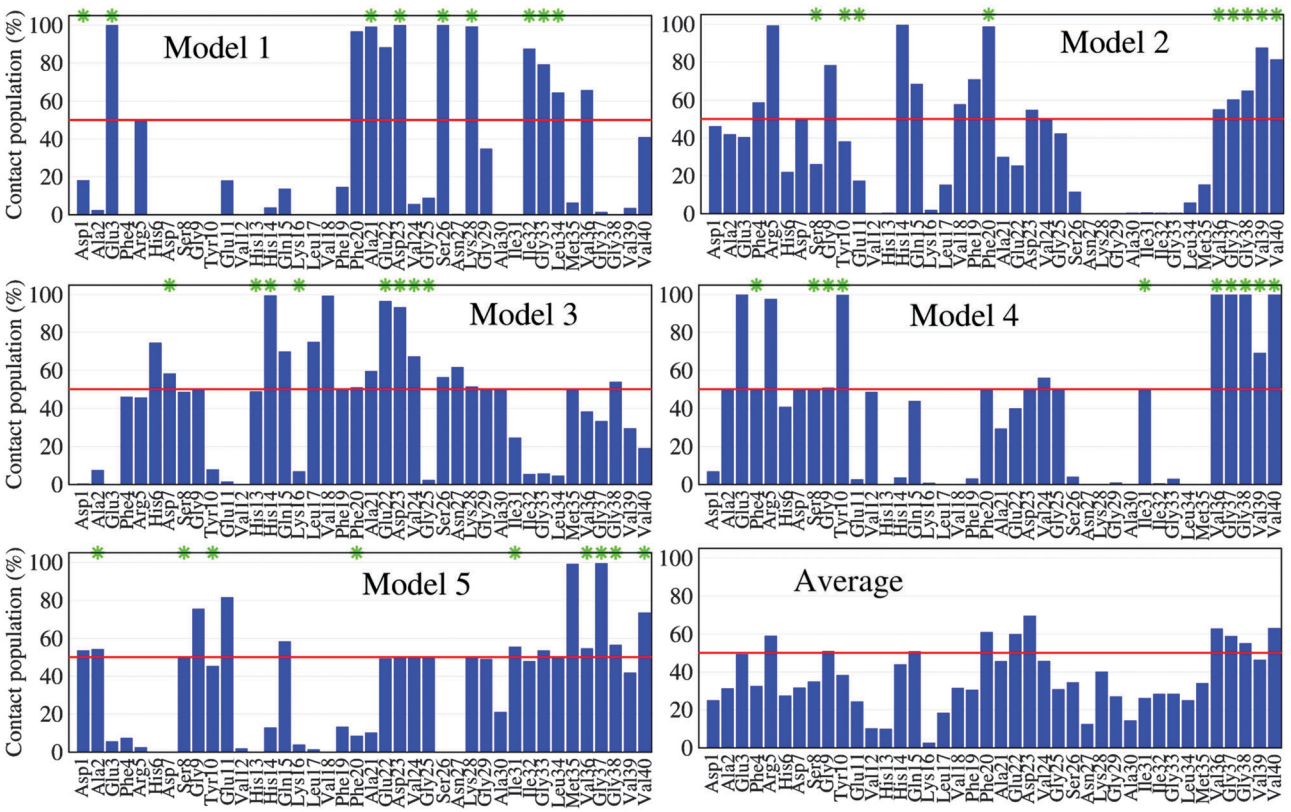

Fig. 7 Probability that an amino acid (AA) stays in contact with isomer L1 of $C_{60}(OH)_{16}$ in equilibrium. AAs with green stars have contact with the ligand in the best docking mode. The red line refers to a probability of 50%, above which the binding is strong.

Table 3 List of residues locating near isomer L1 of $C_{60}(OH)_{16}$.The results were obtained by MD simulations. The adjacent amino acids are defined as those forming contact with fullerenol for more than 50% of the time in equilibrium (Fig. 7)

Model	Residues
1	Glu3, Phe20, Ala21, Glu22, Asp23, Ser26, Lys28, Ile32, Gly33, Leu34, Val36
2	Phe4, Arg5, Asp7, Gly9, His14, Gln15, Val18, Phe19, Phe20, Asp23, Val36, Gly37, Gly38, Val39, Val40
3	His6, Asp7, Gly9, His14, Gln15, Leu17, Val18, Phe19, Phe20, Ala21, Glu22, Asp23, Val24, Ser26, Asp27, Lys28, Gly29, Gly38
4	Ala2, Glu3, Phe4, Arg5, Asp7, Gly9, Tyr10, Phe20, Asp23, Val24, Gly25, Val36, Gly37, Gly38, Val39, Val40
5	Asp1, Ala2, Gly9, Glu11, Gln15, Asp23, Gly25, Ile31, Gly33, Met35, Val36, Gly37, Gly38, Val40

for the initial step in fibril formation (Fig. 7). However, in models 1, 2 and 3 the contact propensity of some residues exceeds 50% and the mean probability is high for Phe20. From this prospect the interaction of L1 with the 17–21 region may also slow $A\beta_{40}$ self-assembly.

Fig. S8 (ESI†) shows the probability of the most unstable isomer L7 being in contact with residues of $A\beta_{40}$ peptide during MD simulations. In the first two models fullerenol weakly binds to the C-terminus but in the last three model the propensity to SC contact formation becomes higher. Moreover, the mean probability of the residues Gly37, Gly38 and Val39 exceeds 50% (Fig. S8, ESI†) implying the important role of this terminus in fullerenol binding. In models 1 and 3, 100% and 50% of equilibrium time fullerenol interacts with Asp23 and Lys28, respectively, while in model 2 these values are 29.7% and 84.2%. In models 4 and 5, where the binding is weak, fullerenol spends much less time near the salt bridge suggesting that locking to the salt bridge Asp23–Lys28 is also crucial for fullerenol binding. In the presence of L7 the Asp23–Lys28 distance increased from 0.83 nm to 0.97 nm suggesting that, as in the L1 isomer case, the inhibition of Aβ aggregation is due to increased flexibility of the salt bridge. Relatively high propensity to interact with the central hydrophobic region 17–21 is seen in models 1 and 5 but not in the remaining models (Fig. S8 and Table S7, ESI†). Thus the role of this hydrophobic region is not as pronounced as in the case of L1.

Taken together, the binding mechanisms of L1 and L7 are similar. Fullerenol may bind to the C-terminus, the 17–21 region and the region around the Asp23–Lys28 salt bridge due to the lack of the well-defined binding pocket.

Negatively charged amino acids play a decisive role in electrostatic interaction with fullerenol

Because of the importance of electrostatic interactions (Table 2), we decomposed it into residues to see which amino acids of $A\beta_{40}$ are the most relevant for binding. For comparison the vdW interactions were also decomposed. Per-residue electrostatic and vdW contributions for the L1 case are shown in Fig. 8. Considering residues which made contribution ≤ -10 kcal mol^{-1} as the most important ones, in model 1 those residues are Glu3 and Asp23

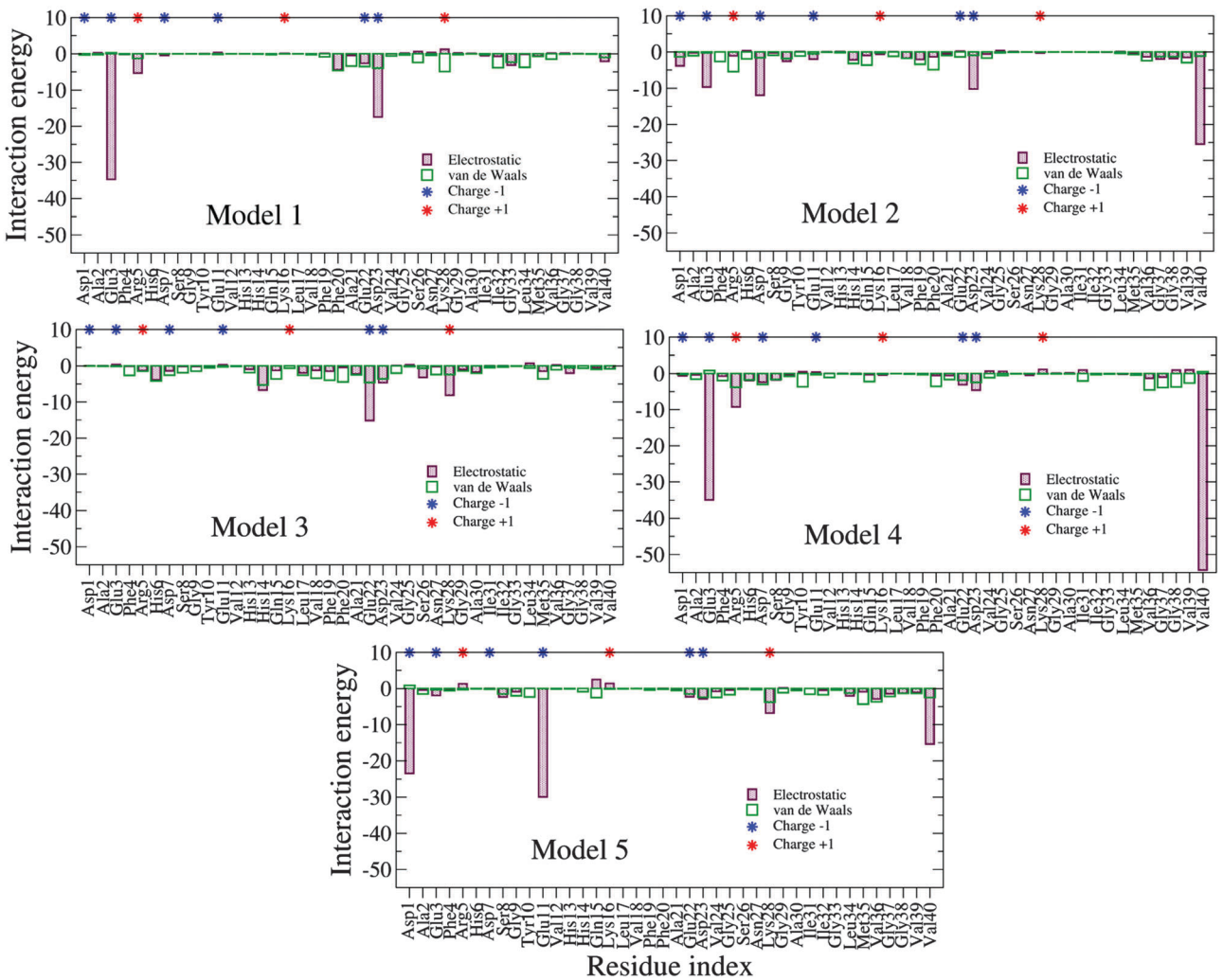

Fig. 8 Per-residue distributions for vdW and Coulomb interactions with the most stable isomer L1 of fullerenol $C_{60}(OH)_{16}$. Results were obtained by MD simulations.

which have charge of $-1e$. In addition to these two residues Asp7 is also crucial in model 2. Residues Glu22 and Glu3 dominate in the electrostatic interaction with $A\beta_{40}$ for model 3 and 4, respectively, while in model 5 these residues are Asp1 and Glu11 (Fig. 8). In models 2, 4 and 5 neutral residue Val40 makes substantial contribution apart from negatively charged residues.

Per-residue electrostatic and vdW contributions are shown in Fig. S9 (ESI†) for isomer L7. In the first three models residues Asp1, Glu3, Asp7, Glu11, Glu22, and Asp23 are dominating. All of these amino acids have a charge of $-1e$, except Lys16 which is positively charged but contributes -16.6 kcal mol^{-1} to the Coulomb interactions (model 3). In models 4 and 5, in addition to the neutral Val40 residue, negatively charged residues Asp7, Glu3 and Glu11 strongly interact with fullerenol $C_{60}(OH)_{16}$ isomer L7. Thus, our simulation suggests that negatively charged amino acids are decisive in binding propensity for both isomers L1 and L7 and, therefore, presumably for any isomers. This is because the negatively charged amino acids like aspartate (Asp) and glutamate (Glu) have a -1 charge at one oxygen atom of COO^- group in side-chain and these oxygen atoms strongly interact with hydrogen atoms at the outermost of $C_{60}(OH)_{16}$. These oxygen atoms as well as other oxygen atoms from COO^- form hydrogen bond with OH groups of $C_{60}(OH)_{16}$ during the most of equilibration time. In the case of van de Waals interactions, none of the amino acids make prominent contributions to the binding propensity (Fig. 8 and Fig. S9, ESI†).

Toxicity of fullerenol $C_{60}(OH)_{16}$

We have tested the cytotoxic effect of fullerenol $C_{60}(OH)_{16}$ on a human neuroblastoma cell line SH-SY5Y, which is commonly used as model cell line for Alzheimer's related studies. The control cells and cells exposed to various fullerenol concentrations (from 0.001 to 50 μg ml^{-1}) were cultured for 24 h and 72 h and the viability of cells was established by WST-1 assay. The dependence of cell viability *vs.* fullerenol concentration is shown in Fig. 9. The 24 h exposure of cells to fullerenol caused no significant changes in viability relative to control at all studied concentrations. After 72 h exposure the cell viability was reduced to 50% of control cells at the highest concentration of fullerenol (50 μg ml^{-1}).

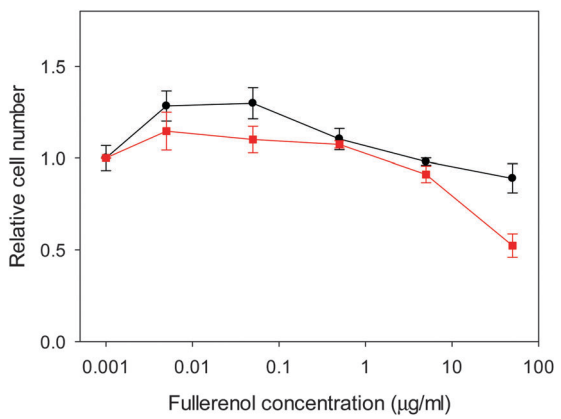

Fig. 9 Viability of the SH-SY5Y cells treated with 0.001–50 μg ml^{-1} fullerenol for 24 h (black circle) and 72 h (red square) determined by WST-1 assay. The data are presented relative to control samples, values correspond to the mean ± SEM (n = 3).

Discussion

The therapeutic potential of fullerenols against oxidative stress-connected processes has been of interest in many studies. Various derivatives of fullerenols were also tested as drug-delivery systems. However, there is a lack of detailed studies for anti-amyloid properties of water-soluble modification of fullerenes with a focus on understanding of mechanism of inhibition.

Recent data indicate that the type of fullerene modification influences their anti-amyloid activities. Kim *et al.* have demonstrated that sodium fullerenolate destroyed mature amyloid fibrils and inhibited aggregation of $A\beta_{42}$ peptide for a 1 : 1 (w/w) ratio (at peptide concentration of 0.1 mg ml^{-1}).[55] Kim and Lee showed that (dimethoxymethano)fullerene inhibited aggregation of both $A\beta_{42}$ peptide and its fragment $A\beta_{11-25}$ with IC_{50} constant at ~9 μM.[21] Another group has investigated anti-amyloid activity of fullerene–polyvinylpyrrolidone (PVP) complexes and sodium salt of a polycarboxylic derivative of fullerene (NaFH) on $A\beta_{42}$ peptide amyloid fibrils and fibrils formed from muscle X-protein. They found out that the most effective were the fullerene–polyvinylpyrrolidone complexes.[56] The differences in anti-amyloid activities of fullerene derivatives may be also due to different scaffolds leading to different sizes of fullerene molecules. Xiu *et al.* have compared the inhibitory effect of fullerene C_{180} with 180 carbon atoms in the scaffold with the same number of carbon atoms but a smaller surface area, namely with three C_{60} molecules ($3C_{60}$). They found out that C_{180} had a much stronger inhibitory effect on $A\beta_{16-22}$ fibril formation.[57] The obtained results suggest that fullerene surface modification together with volume/surface ratio play an important role in their anti-amyloid activities.

Our results demonstrate that fullerenol $C_{60}(OH)_{16}$, fullerene C_{60} modified with 16 OH groups, is able to influence the amyloid aggregation of $A\beta_{40}$ peptide. Both the experimental and computational results showed that $C_{60}(OH)_{16}$ inhibits fibrillization of $A\beta_{1-40}$ peptide in a dose-dependent manner with half maximal inhibition constant in a very low range (IC_{50} ~ 31.9 μg ml^{-1}). In addition, an *in silico* approach reveals that the inhibition of β-sheet formation by $C_{60}(OH)_{16}$ results from the strong electrostatic interactions of the fullerenol OH groups with the polar, negatively charged amino acids. The strong interactions between the fullerenol and $A\beta_{40}$ peptides significantly weaken the peptide–peptide interaction that is important for β-sheet formation, and thus inhibit $A\beta_{40}$ fibrillization. In most theoretically studied models the tight fullerenol binding is due to interaction with the D23–K28 salt bridge, which also plays a crucial role in formation of fibril cross-beta structures.

The evaluation of fullerenol biocompatibility was found to be of great importance. Several studies have reported the dependence of fullerenol cytotoxicity related to several parameters, like cell-type, degree of fullerene hydroxylation, concentration or time

of administration. Cell types from different species and different pathologies were used to investigate fullerenol cytotoxicity. The range of cell models varied from normal animal cells (Chinese hamster lung, Chinese hamster ovary cells and L929 mouse subcutaneous connective cells, LLC-PK1 porcine proximal tubule kidney) to normal human (human epidermal keratinocytes) and human cancer (hepatocellular carcinoma HepG2, colorectal adenocarcinoma Caco-2) cell types.[26–28,58] A comparison between the sensibility of all these cell lines to fullerenol is difficult to carry out since they have different origins, however the normal human epidermal keratinocytes were more sensitive to fullerenol (decrease of cell viability observed from 42.5 μg ml^{-1} fullerenol for 24 h) compared to normal animal cells (cytotoxicity started from 75 μg ml^{-1} fullerenol).[28,59] The higher degree of fullerene hydroxylation was associated with increased cytotoxicity. Thus, rat hepatocytes exposed for 1 h to fullerenol (x = 24) led to a significant decrease of cell viability to 10% compared to fullerenol (x = 12) where the viability was 75%.[59] Similarly, the increase of the hydroxylation degree of fullerenol (x = 32) was correlated with decreased viability in human epidermal keratinocytes after 24 h of exposure.[28] A direct dependency of the decrease in viability and increase in fullerenol concentration was noticed in several studies. Concentrations higher than 6 mM of fullerenol derivative $C_{60}(OH)_{15}(ONa)_9(H_2O)_{15}$ were toxic for LLC-PK1 porcine proximal tubule kidney cells.[26] Finally, the cytotoxity was increased when the longer exposure to fullerenol was applied. Human hepatocellular carcinoma HepG2 cell line and human colorectal adenocarcinoma Caco-2 cell lines exposed to fullerenol displayed time-dependent decreased viability with almost no changes at 12 h and reduction to 53% and 38% at 96 h.[58] Other human hepatocellular carcinoma SMCC-7721 cell lines displayed reduced viability by 50% at 72 h exposure to fullerenol.[60] Due to increased heterogeneity of the proposed cell models a final conclusion will be difficult to state. However, according to the already reported data, an exposure time longer than 48 h associated with fullerenol doses higher than 40 μg ml^{-1} and an increased number of hydroxyl groups have been associated with amplified cytotoxicity. Our results showed that modification of the fullerene surface with 16 hydroxyl groups caused no significant effect on viability of SH-SY5Y human neuroblastoma cell line at 24 h for all investigated concentrations and at 72 h for concentrations below 50 μg ml^{-1}. These data indicate that fullerenol $C_{60}(OH)_{16}$ was not toxic for the SH-SY5Y neuroblastoma cell line at a concentration able to affect Aβ peptide amyloid fibrillization, namely at a fibrillization IC_{50} constant value equal to 31.9 μg ml^{-1}.

Conclusion

In this study we have investigated the interaction of the fullerene C_{60} modified with 16 OH groups with $A\beta_{40}$ amyloid fibrillization. It was observed that $C_{60}(OH)_{16}$ effectively reduces the formation of amyloid fibrils. The IC_{50} value of 31.9 μg ml^{-1} is in the low range and suggests that fullerenol interferes with $A\beta_{40}$ aggregation at stoichiometric concentrations. The *in silico* calculation revealed that fullerenol $C_{60}(OH)_{16}$ tightly binds to $A\beta_{40}$. The electrostatic interaction dominantly contributes to the binding propensity *via* the interaction of oxygen atoms from the COO^- groups of side chains of polar, negatively charged amino acids with the OH groups of fullerenol. Our analysis revealed the diversity of the binding pathways and binding poses. Due to the lack of a well-defined binding pose, fullerenol may bind to residues Asp23 and Lys28 as well as to the C-terminus and the main hydrophobic patch (LVFFA). More importantly, comparing the distance between Asp23 and Lys28 obtained by MD simulations of $A\beta_{40}$–fullerenol complexes with that obtained from initial structures of five models it was shown that upon fullerenol binding the salt bridge becomes more flexible (the Asp23–Lys28 distance becomes larger). On the other hand, as shown in the pioneering experimental work of Sciarretta *et al.*[52] the fixation of this distance considerably speeds up the $A\beta_{40}$ fibril formation. From this perspective, fullerenol can interfere with aggregation through enhanced flexibility of the salt bridge.

Investigation of the effect of fullerenol on the viability of the human neuroblastoma SH-SY5Y cell line suggested that $C_{60}(OH)_{16}$ was not toxic for neuroblastoma cells at concentrations which are able to effectively inhibit Aβ peptide amyloid fibrillization.

The obtained results suggested that fullerenol $C_{60}(OH)_{16}$ represents a promising candidate of therapeutics for Alzheimer's disease due to its ability to inhibit amyloid fibrils formation in its early stages by binding to monomer $A\beta_{40}$, namely through the interactions with polar, negatively charged amino acids. Further work with animal models for neurodegenerative diseases will be required to test the efficacy of fullerenol *in vivo*.

Acknowledgements

This work was supported by VEGA projects 2/0181/13, 2/0176/14, MVTS-COST 083/14 action BM1405 and EU grant 26220220005. M. S. L. and P. D. Q. H. were supported by Vietnam National Foundation for Science and Technology Development (NAFOSTED) under grant number 106-YS.02-2013.01, Department of Science and Technology at Ho Chi Minh city, Vietnam and Polish NCN grant 2015/19/B/ST4/02721. Allocation of CPU time at the supercomputer center TASK in Gdansk (Poland) is highly appreciated.

Notes and references

1 R. Yan and R. Vassar, *Lancet Neurol.*, 2014, **13**, 319–329.
2 K. A. DaSilva, J. E. Shaw and J. McLaurin, *Exp. Neurol.*, 2010, **223**, 311–321.
3 M. H. Viet, C.-Y. Chen, C.-K. Hu, Y.-R. Chen and M.-S. Li, *PLoS One*, 2013, **8**, e79151.
4 S. T. Ngo and M. S. Li, *Mol. Simul.*, 2013, **39**, 279–291.
5 Q. V. Vuong, Z. Bednarikova, A. Antosova, P. D. Q. Huy, K. Siposova, N. A. Tuan, M.S. Li and Z. Gazova, *MedChemComm*, 2015, **6**, 810–822.
6 Q. V. Vuong, K. Siposova, T. T. Nguyen, A. Antosova, L. Balogova, L. Drajna, J. Imrich, M. S. Li and Z. Gazova, *Biomacromolecules*, 2013, **14**, 1035–1043.

7 M. H. Viet, K. Siposova, Z. Bednarikova, A. Antosova, T. T. Nguyen, Z. Gazova and M. S. Li, *J. Phys. Chem. B*, 2015, **119**, 5145–5155.
8 K. L. Sciarretta, D. J. Gordon and S. C. Meredith, *Methods Enzymol.*, 2006, **413**, 273–312.
9 A. Bellova, E. Bystrenova, M. Koneracka, P. Kopcansky, F. Valle, N. Tomasovicova, M. Timko, J. Bagelova, F. Biscarini and Z. Gazova, *Nanotechnology*, 2010, **21**, 065103.
10 K. Siposova, M. Kubovcikova, Z. Bednarikova, M. Koneracka, V. Zavisova, A. Antosova, P. Kopcansky, Z. Daxnerova and Z. Gazova, *Nanotechnology*, 2012, **23**, 055101.
11 A. Antosova, Z. Gazova, D. Fedunova, E. Valusova, E. Bystrenova, F. Valle, Z. Daxnerova, F. Biscarini and M. Antalik, *Mater. Sci. Eng., C*, 2012, **32**, 2529–2535.
12 S. Mirsadeghi, S. Shanehsazzadeh, F. Atyabi and R. Dinarvand, *Mater. Sci. Eng., C*, 2016, **59**, 390–397.
13 H. W. Kroto, J. R. Heath, S. C. O'Brien, R. F. Curl and R. E. C. Smalley, *Nature*, 1985, **318**, 162–163.
14 L. Xiao, H. Aoshima, Y. Saitoh and N Miwa, *Free Radical Biol. Med.*, 2011, **51**, 1376–1389.
15 L. L. Dugan, D. M. Turetsky, C. Du, D. Lobner, M. Wheeler, C. R. Almli, C.K.-F. Shen, T.-Y. Luh, D. W. Choi and T.-S. Lin, *Proc. Natl. Acad. Sci. U. S. A.*, 1997, **94**, 9434–9439.
16 J. Grebowski, P. Kazmierska and A. Krokosz, *BioMed Res. Int.*, 2013, **2013**, 751913.
17 R. S. Ruoff, D. S. Tse, M. Malhotra and D. C. Lorents, *J. Phys. Chem.*, 1993, **97**, 3379–3383.
18 S. Bosi, T. Da Ros, G. Spalluto and M. Prato, *Eur. J. Med. Chem.*, 2003, **38**, 913–923.
19 S. H. Friedman, D. L. DeCamp, R. P. Sijbesma, G. Srdanov, F. Wudl and G. L. Kenyon, *J. Am. Chem. Soc.*, 1993, **115**, 6506–6509.
20 C. Chen, G. Xing, J. Wang, Y. Zhao, B. Li, J. Tang, G. Jia, T. Wang, J. Sun, L. Xing, H. Yuan, Y. Gao, H. Meng, Z. Chen, F. Zhao, Z. Chai and X. Fang, *Nano Lett.*, 2005, **5**, 2050–2507.
21 J. E. Kim and M. Lee, *Biochem. Biophys. Res. Commun.*, 2003, **303**, 576–579.
22 I. Y. Podolski, Z. A. Podlubnaya, E. A. Kosenko, E. A. Mugantseva, E. G. Makarova, L. G. Marsagishvili, M. D. Shpagina, Y. G. Kaminsky, G. V. Andrievsky and V. K. Klochkov, *J. Nanosci. Nanotechnol.*, 2007, **7**, 1479–1485.
23 A. G. Bobylev, L. G. Marsagishvili, M. D. Shpagina, V. S. Romanova, R. A. Kotelnikova and Z. A. Podlubnaya, *Biofizika*, 2010, **55**, 394–399.
24 L. G. Marsagishvili, A. G. Bobylev, M. D. Shpagina and Z. A. Podlubnaya, *Abstr. XXXVIII Europ. Muscle Conf.*, Lille, France, 2009.
25 A. G. Bobylev, L. G. Marsagishvili, M. D. Shpagina and Z. A. Podlubnaya, *Abstr. XXXVIII Europ. Muscle Conf.*, Lille, France, 2009.
26 D. N. Johnson-Lyles, K. Peifley, S. Lockett, B. W. Neun, M. Hansen, J. Clogston, S. T. Stern and S. E. McNeil, *Toxicol. Appl. Pharmacol.*, 2010, **248**, 249–258.
27 Y. Su, J. Y. Xu, P. Shen, J. Li, L. Wang, Q. Li, W. Li, G. T. Xu, C. Fan and Q. Huang, *Toxicology*, 2010, **269**, 155–159.
28 J. G. Saathoff, A. O. Inman, X. R. Xia, J. E. Riviere and N. A. Monteiro-Riviere, *Toxicol. In Vitro*, 2011, **25**, 2105–2112.
29 Y. Y. Zha, B. Yang, M. L. Tang, Q. C. Guo, J. T. Chen, L. P. Wen and M. Wang, *Int. J. Nanomed.*, 2012, **7**, 3099–3109.
30 S. Wang, P. He, J. M. Zhang, H. Jiang and S. Z. Zhu, *Synth. Commun.*, 2005, **35**, 1803–1808.
31 H. Q. He, L. M. Zheng, P. Jin and M. H. Yang, *Comput. Theor. Chem.*, 2011, **974**, 16–20.
32 M. J. Frisch, *et al.*, *Gaussian 09, Revision D.01*, Gaussian, Inc., Wallingford, CT, 2013.
33 R. Dennington, T. Keith and J. Millam, *GaussView Version 5*, Semichem Inc., Shawnee Mission KS, 2009.
34 M. J. Frisch, *et al.*, *Gaussian 09 Revision D.01*, Gaussian Inc., Wallingford, CT, 2009.
35 V. Hornak, R. Abel, A. Okur, B. Strockbine, A. Roitberg and C. Simmerling, *Proteins: Struct., Funct., Bioinf.*, 2006, **65**, 712–725.
36 J. Wang, R. M. Wolf, J. W. Caldwell, P.A. Kollman and D. A. Case, *J. Comput. Chem.*, 2004, **25**, 1157–1174.
37 J. Wang, W. Wang, P. A. Kollman and D. A. Case, *J. Mol. Graphics Modell.*, 2006, **25**, 247–260.
38 A. Jakalian, D. B. Jack and C. I. Bayly, *J. Comput. Chem.*, 2002, **23**, 1623–1641.
39 P. D. Q. Huy, Y.-C. Yu, S. T. Ngo, T. V. Thao, C. Piao Chen, M. S. Li and Y.-C. Chen, *Biochim. Biophys. Acta, Gen. Subj.*, 2013, **1830**, 2960–2969.
40 M. Sanner and F. Python, *J. Mol. Graphics Modell.*, 1999, **17**, 57–61.
41 O. Trott and A. J. Olson, *J. Comput. Chem.*, 2010, **31**, 455–461.
42 I. Klapper, R. Hagstrom, R. Fine, K. Sharp and B. Honig, *Proteins: Struct., Funct., Bioinf.*, 1986, **1**, 47–59.
43 J. Warwicker and H. Watson, *J. Mol. Biol.*, 1982, **157**, 671–679.
44 W. L. Jorgensen, J. Chandrasekhar, J. D. Madura, R. W. Impey and M. L. Klein, *J. Chem. Phys.*, 1983, **79**, 926935.
45 D. A. Case, *et al.*, *AMBER 12*, 2012, http://ambermd.org/.
46 P. D. Q. Huy and M. S. Li, *Phys. Chem. Chem. Phys.*, 2014, **16**, 20030–20040.
47 L. H. Lu, Y. T. Lee, H. W. Chen, L. Y. Chiang and H. C. Huang, *Br. J. Pharmacol.*, 1998, **123**, 1097.
48 I. Y. Podolsky, E. V. Kondratjeva, S. S. Gurin, M. A. Dumpis and L. B. Piotrovsky, *Fullerenes, Nanotubes, Carbon Nanostruct.*, 2005, **12**, 421.
49 J. Nasica-Labouze, P. H. Nguyen, F. Sterpone, O. Berthoumieu, N. V. Buchete, S. Coté, A. De Simone, A. J. Doig, P. Faller, A. Garcia, A. Laio, M. S. Li, S. Melchionna, N. Mousseau, Y. Mu, A. Paravastu, S. Pasquali, D. J. Rosenman, B. Strodel, B. Tarus, J. H. Viles, T. Zhang, C. Wang and P. Derreumaux, *Chem. Rev.*, 2015, **115**, 3518–3563.
50 M. H. Viet, S. T. Ngo, N. S. Lam and M. S. Li, *J. Phys. Chem. B*, 2011, **115**, 7433–7446.
51 S. T. Ngo and M. S. Li, *J. Phys. Chem. B*, 2012, **116**, 10165–10175.
52 K. L. Sciarretta, D. J. Gordon, A. T. Petkova, R. Tycko and S. C. Meredith, *Biochemistry*, 2005, **44**, 6003–6014.
53 G. Reddy, J. E. Straub and D. Thirumalai, *J. Phys. Chem. B*, 2009, **113**, 1162–1172.

54 M. H. Viet, P. H. Nguyen, S. T. Ngo, M. S. Li and P. Derreumaux, *ACS Chem. Neurosci.*, 2013, **4**, 1446–1457.
55 A. G. Bobylev, A. B. Kornev, L. G. Bobyleva, M. D. Shpagina, I. S. Fadeeva, R. S. Fadeev, D. G. Deryabin, J. Balzarini, P. A. Troshin and Z. A. Podlubnayaa, *Org. Biomol. Chem.*, 2011, **9**, 5714–5719.
56 A. G. Bobylev, M. D. Shpagina, L. G. Bobyleva, A. D. Okuneva, L. B. Piotrovsky and Z. A. Podlubnaya, *Biofizika*, 2012, **57**, 416–421.
57 L. Xie, Y. Luo, D. Lin, W. Xi, X. Yang and G. Wei, *Nanoscale*, 2014, **6**, 9752–9762.
58 R. Injac, M. Perse, N. Obermajer, V. Djordjevic-Milic, M. Prijatelj, A. Djordjevic, A. Cerar and B. Strukelj, *Biomaterials*, 2008, **29**, 3451–3460.
59 Y. Nakagawa, T. Suzuki, H. Ishii, D. Nakae and A. Ogata, *Arch. Toxicol.*, 2011, **85**, 1429–1440.
60 Y. Liu, Z. Wang and X. Wang, *J. Mech. Behav. Biomed. Mater.*, 2015, **45**, 65–74.